SLAC-PUB-7199
June 1996

PRELIMINARY MEASUREMENTS OF PRODUCTION OF $\pi^{\pm}, K^{\pm}, p, K^0$ and Λ^0 IN HADRONIC Z^0 DECAYS*

The SLD Collaboration**
Stanford Linear Accelerator Center
Stanford University, Stanford, CA 94309

*This work was supported by Department of Energy contracts: DEFG02-91ER40676 (BU), DE-FG03-92ER40701 (CIT), DE-FG03-91ER40618 (UCSB), DE-FG03-92ER40689 (UCSC), DE-FG03-93ER40788 (CSU), DE-FG02-91ER40672 (Colorado), DEFG02-91ER40677 (Illinois), DE-AC03-76SF00098 (LBL), DBFG02-92ER40715 (Massachusetts), DE-AC02-76ER03069 (MIT), DE-FG06-85ER40224 (Oregon), DE-AC03-76SF00515 (SLAC), DE-FG05-91ER40627 (Tennessee), DE-AC02-76ERO0881 (Wisconsin), DE-FG02-92ER40704 (Yale); National Science Foundation grants: PHY-91-13428 (UCSC), PHY-89-21320 (Columbla), PHY-92-04239 (Cincinnati), PHY-88-17930 (Rutgers), PHY-88-19316 (Vanderbilt), PHY-92-03212 (Washington); the UK Science and Engineering Research Council (Brunel and RAL); the Istituto Nazionale di Fisica Nucleare of Italy (Bologna, Ferrara, Frascati, Pisa, Padova, Perugia); and the Japan-US Cooperative Research Project on High Energy Physics (Nagoya, Tohoku).

Ref PA04-045
Submitted to the 28th International Conference on High Energy Physics, Warsaw, Poland, July 25-31, 1996

A B S T R A C T

We have measured production of $\pi^{\pm}, K^{\pm}, p/\bar{p}, K^0$ and $\Lambda^0/\bar{\Lambda}^0$ as a function of momentum in inclusive hadronic Z^0 decay events and separately in events containing primary light - *(uds)* and *b*- quarks. The SLD Cherenkov Ring Imaging Detector was used to identify charged pions, kaons and protons over most oft he available momentum range 0.8< p < 33 GeV/c. The neutral K^0_s and Λ^0 were reconstructed using the $\pi^+\pi^-$ and $p\pi^-$ decay modes, respectively. We present the first comparisons of momentum distributions in primary light- and *b*- flavor events, tagged using impact parameters of charged tracks measured in the SLD Vertex Detector. Substantial differences are observed, consistent with the kinematics of *B*- hadron production in Z^0 decays and the properties of *B*- hadron decays as measured at lower energies.

1 Introduction

The production of jets of final state hadrons from partons is currently believed to proceed in three stages. Considering the process $e^+e^- \to Z^0 \to q\bar{q}$, the first stage involves the radiation of gluons from the primary quark and antiquark, which in turn may radiate gluons or split into $q\bar{q}$ pairs until their virtuality approaches the hadron mass scale. Such a 'parton shower" is calculable in perturbative QCD, for example [1]. The second stage, in which these partons transform into 'primary" hadrons, is not understood quantitatively, although several hadronization models exist.

Measurements of the production rates and momentum distributions of identified particles are useful for probing the hadronization process, since the mass of the primary hadron may influence the dynamics. However the third stage, in which unstable primary hadrons decay into stable hadrons, complicates the interpretation of inclusive measurements. It is desirable to remove the effects of these decays when testing the predictions of theory or hadronization models. Additional complications arise in jets initiated by heavy quarks, in which the leading heavy hadrons carry a large fraction of the beam energy, restricting that available to other primary particles, and their decays produce a sizable fraction of the stable particles in the jet.

In this paper we present an analysis of $\pi^\pm$, $K^\pm$, $p/\bar{p}$, K^0, and $\Lambda^0/\bar{\Lambda}^0$ production in hadronic Z^0 decays collected by the SLC Large Detector (SLD). The analysis is based upon the approximately 150,000 hadronic events collected in runs of the SLAC Linear Collider (SLC) between 1993 and 1995. We measured production rates as a function of momentum in an inclusive sample of all hadronic events and also in high-purity samples of light- $(Z^0 \to u\bar{u}, d\bar{d}, s\bar{s})$ and *b*- $(Z^0 \to b\bar{b})$ tagged events. From these three samples we extracted momentum distributions in light- and *b*- flavor events. The unfolded momentum distributions for the light-flavor events are free from effects of heavy quark production and decay. Although the influence of decay products of other unstable primary hadrons remains, these measurements are more appropriate for comparison with QCD predictions, which generally assume massless quarks.

2 The SLD and Hadronic Event Selection

This analysis used charged tracks measured in the SLD Central Drift Chamber (CDC) [2] and silicon Vertex Detector (VXD) [3]. The CDC consists of 80 layers of sense wires arranged in 10 axial or stereo superlayers. Momentum measurement is provided by a uniform axial magnetic field of 0.6 T. The VXD is composed of charge-coupled devices containing a total of 120 million 22x 22 μm^2 pixels arranged in four concentric layers of radius between 2.9 and 4.2 cm. Including the uncertain y on the primary interaction point (IP), the CDC and VXD give a combined 2D-impact parameter resolution of $11 \oplus 76/(p_\perp \sqrt{\sin\theta})\,\mu m$, where $p_\perp$ is the track momentum transverse to the beam axis in GeV/c.

Identification of charged particles is accomplished with the barrel portion of the Cherenkov Ring Imaging Detector (CRID) [4], which covers the polar angle range $|\cos\theta| \leq 0.68$. Through the use of liquid C_6F_{14} and gaseous C_5F_{12} radiators, the CRID is designed to provide efficient charged $\pi/K/p$ identification over most of the available momentum range up to 45 GeV/c. A charged particle that passes through a radiator of refractive index n with velocity above Cherenkov threshold, $\beta > \beta_0 = 1/n$, emits photons at an angle $\theta_c = \cos^{-1}(1/\beta n)$ with respect to its flight direction. Such photons are imaged through quartz windows into time projection chambers (TPCs) containing a photosensitive gas. The resulting photoelectrons drift to wire chambers where the conversion point of each is measured in three dimensions using drift time, wire address and charge division. These positions are used to reconstruct a Cherenkov angle with respect to each extrapolated charged track.

The liquid (gas) radiator index of refraction was measured to be 1.282 (1.00172), corresponding to Cherenkov thresholds for charged pions, kaons and protons of 0.17, 0.62 and 1.17 (2.4, 8.4 and 16.0) GeV/c, respectively. The average number of detected photons was 10.5 (9.2) per full ring for tracks with β = 1. The average Cherenkov angle resolution was 16 (4.5) mrad including the effects of residual misalignments and track extrapolation resolution. The local or intrinsic resolution was 13 (3.8) mrad, consistent with the design value. The particle identification performance of the barrel CRID is described in the next section.

The trigger and initial selection of hadronic events are described in [5]. The analysis presented here is based on charged tracks measured in the CDC and VXD. A set of

cuts was applied in order to select events well-contained within the detector acceptance. Tracks were required to have (i) a closest approach to the beam axis within 1 cm, and within 5 cm along the beam axis of the measured interaction point, (ii) a polar angle θ with respect to the beam axis with $|\cos\theta| < 0.80$, (iii) a minimum momentum transverse to this axis of $p_\perp > 200$ MeV/c, and (iv) a maximum momentum of $p < 50$ GeV/c. Events were required to contain a minimum of seven such tracks, a thrust [6] axis polar angle with respect to the beam axis θ_T within $|\cos\theta_T| < 0.71$, and a minimum charged visible energy $E_{vis} > 18$ GeV, with all tracks assigned the charged pion mass. In addition, events were required to have at least three tracks linked to VXD hits, and to have a well-measured IP position [7]. A sample comprising 90,213 events passed these cuts.

Samples of events enriched in light and *b* primary flavors were selected based on impact parameters δ of charged tracks with respect to the IP in the plane transverse to the beam [7]. For each event we define n_{sig} to be the number of tracks pasing a set of quality cuts that have impact parameter greater than three times its estimated error, $\delta > 3\sigma_\delta$. Events with $n_{sig} = 0$ were assigned to the light-tagged sample and those with $n_{sig} \geq 3$ were assigned to the *b*- tagged sample. The light- and *b*- tagged samples comprised 53,526 and 14,039 events, with purities of 86% and 90%, respectively, estimated from our Monte Carlo simulation [7].

3 Charged Hadron Identification

Charged π, *K* and *p* were identified using the 78,215 events for which the CRID was operational. Information from the liquid and gas radiators was analyzed separately, the liquid being used for tracks with momentum below 6 GeV/c and the gas for tracks with momentum above 3 GeV/c. Additional track selection cuts were applied to remove tracks that might have scattered through large angles before exiting the CRID and to ensure that the CRID performance was well-modelled by our detector simulation. Tracks were required to have (i) at least 40 CDC hits, at least one of which was in the outermost superlayer, (ii) to extrapolate through an active region of the appropriate radiator, and (iii) to have at least 80 (100)% of their expected liquid (gas) ring contained within a sensitive region of the CRID TPCs. For the gas analysis, the latter requirement

included rejection of tracks for which there was a saturated hit from passage of a charged particle within 5 cm of the expected gas ring center. For the liquid analysis, tracks were required to have a saturated hit within 1 cm of the extrapolated track. For the gas analysis, either such a saturated hit or the presence of at least four hits consistent with a liquid ring was required. These cuts accepted 47% and 43% of tracks within the barrel acceptance for the liquid and gas analysis, respectively.

We measured the fractions of the selected tracks that were identified as π, K and p in a series of momentum bins. Electrons and muons were not distinguished from pions. This background was estimated from the Monte Carlo simulation [7] to comprise about 5% of the inclusive track sample, and a correction was applied. The fractions were also corrected for the effects of beam-related backgrounds, particles interacting in the detector material, and particles decaying outside the detector acceptance, using the simulation, such that only charged pions, kaons and protons from the primary interaction or from decays of particles with lifetime less than 3×10^{-10}s were counted. For momenta below 2 GeV/c, only negatively charged tracks were used since protons from interactions in the detector material are predominantly positive and have relatively low momentum.

Tracks were identified using a likelihood technique [8]. For each of the three charged hadron hypotheses $i = \pi, K, p$, a likelihood L_i was calculated based upon the number of detected photoelectrons and their measured angles, the expected number of photons, the expected Cherenkov angle, and a background term. The background included the effects of overlapping Cherenkov radiation from other tracks in the event as well as a constant term normalized to the number of hits in the TPC in question that were not associated with any track. Particle separation was based upon differences between logarithms of these three likelihoods, $\mathcal{L}_i = \ln L_i$. For the liquid (gas) analysis, we define a particle to be identified as type j, where $j = \pi, K$ or p, if $\mathcal{L}_j$ exceeds both of the other log-likelihoods by at least 5 (3) units.

Efficiencies for identifying particles of type i as type j were determined where possible from the data [9]. Tracks from selected $K^0 \to \pi^+\pi^-$ decays in hadronic events and from $Z^0 \to \tau^+\tau^-$ events in the data were used as 'pion" test samples, with non-$e/\mu/\pi$ contents estimated to be 0.3% and 1.7%, respectively. Figure 1 shows the probability for these tracks to be identified as pions, kaons and protons. Also shown are results of the same analysis applied to corresponding samples from Monte Carlo

simulations subjected to a detailed simulation of the CRID response. The simulation describes the momentum dependence well and reproduces the measured efficiencies to within ± 0.03.

Functional forms were chosen that described the momentum dependence of the efficiencies for both data and simulated test samples, as well as for simulated true pions in $Z^0 \to q\bar{q}$ events, and were fitted to each of these samples. The efficiencies for tracks in the simulated test samples are slightly different from those for simulated pions in $Z^0 \to q\bar{q}$ events due to their non-pion content and their different average momentum and dip angle resolutions. The difference between fitted parameter values in these two simulated samples was added to the fitted values for the data sample to derive corrected $\pi \to j$ identification efficiency functions, which are shown in the leftmost column of Fig. 2. Parameters derived from the K, and τ samples are consistent in their region of overlap, $3 < p < 10$ GeV/c.

The $p \to j$ identification efficiencies, as well as the π-K separation for particles between π- and K- thresholds in the gas ($3 < p < 10$ GeV/c), were measured using protons from Λ^0 decays. In addition, the π-p separation in the liquid (gas) was measured for momenta above 2 (17) GeV/c using the K, and τ test samples. The simulation was used to convert this π-p separation into a $p \to p$ identification efficiency, giving results in agreement with those using Λ^0 decays. The latter analysis had better precision and was therefore used in the appropriate momentum ranges.

The $K \to j$ identification efficiencies were derived by scaling the measured $\pi \to \pi$ identification efficiency by a parametrization of the ratio of simulated $K \to K$ to $\pi \to \pi$ identification efficiencies. For momenta in the ranges $1.5 < p < 2.5$ and $15 < p < 25$ GeV/c, the scale factor was unity. For the $K \to \pi$ and $K \to p$ identification efficiencies, the simulated values were parametrized and the resulting function scaled by the ratio of data to simulated $p \to \pi$ and $\pi \to p$ identification efficiencies, respectively.

These identification efficiencies are shown in Fig. 2 as bands, where the half-widths represent our estimates of their uncertainties. For the diagonal $(i \to i)$ cases, as well as the $\pi \to j$ cases, these correspond to statistical errors on the fitted parameters from the data test samples and are completely positively correlated between momenta in each of the liquid and gas analyses. For the remaining off-diagonal (misidentification) cases a more conservative 25% relative error was assigned at all points to account for the limited experimental constraints on the momentum dependence. In addition,

a minimum absolute uncertainty of ± 0.01 was applied to the cases without a direct experimental measurement. These errors are also strongly positively correlated between momenta.

The correct identification efficiencies in Fig. 2 peak near or above 90% and the pion coverage is continuous from 0.5 GeV/cup to approximately 33 GeV/c. There is a gap in the kaon-proton separation between 6 and 10 GeV/c, and the proton coverage extends all the way to the beam energy. Misidentification rates in the liquid (gas) are typically less than 3 (5)%.

4 Charged Hadron Fractions

For each momentum bin, the number of observed particles of a given type j was related to the true production fraction of particles of type i by an efficiency matrix, composed of the values in Fig. 2 for that bin. This matrix was inverted and used to unfold our observed identified particle rates. This analysis procedure does not require that the sum of the charged particle fractions be unity; instead the sum was used as a consistency check and was found to be within statistical errors of unity for all momenta.

The measured charged particle fractions for hadronic Z^0 decays are shown in Fig. 3 as a function of momentum. In some momentum regions we cannot distinguish two of the three species, so we present only the fraction of the identifiable species, i.e. protons in the liquid above 3 GeV/c and pions in the gas below 10 GeV/c. The errors on the points below 15 GeV/c are dominated by the systematic uncertainties on the identification efficiencies and are strongly positively correlated across the entire momentum range. For $p > 15$ GeV/c the errors have roughly equal statistical and systematic contributions, and the systematic errors are positively correlated and increase in magnitude with momentum. The region above 33 GeV/c was excluded due to limited statistics.

Pions are seen to dominate the charged hadron production at low momentum and to decline steadily toward a fraction of 0.5 as $p \rightarrow p_{beam} = 45.6$ GeV/c, although the data do not exclude a constant fraction above 20 GeV/c. The kaon fraction rises steadily with momentum from less than 0.1 at $p = 1$ GeV/c, approaching the pion fraction at very high momentum. The proton fraction also rises at low momentum, levels off near

0.1 by about 10 GeV/c, and then declines above 20 GeV/c. Where the momentum coverage overlaps, these measured fractions were found to be in agreement with previous measurements at the Z^0 [10, 11, 12]. Measurements based on ring imaging (this measurement and [10]) and those based on ionization energy loss rates [11, 12] cover complementary moment urn ranges and can be combined to provide continuous coverage over the range $0.2 < p < 35$ GeV/c. Also shown in Fig. 3 are the predictions of the JETSET7.4 [13] and HERWIG5.7 [14] event generators using default parameters. The momentum dependence of all three fractions is reproduced by the JETSET model, as is the normalization of the pion fraction. However the predicted proton fraction is higher than that measured in the data and the predicted kaon fraction is lower. The HERWIG model provides a good description of all three fractions at momenta below about 4 GeV/c and of the pion fraction above about 10 GeV/c. However the pion fraction is higher than that in the data for $4 < p < 10$ GeV/c, and the proton fraction is higher above 10 GeV/c.

5 Neutral V^0 Production

To measure the production of $\Lambda^0/\bar{\Lambda}^0$ and K^0 [15], all pairs of oppositely-charged tracks were considered as "V^0" candidates if both tracks had (i) at least 40 hits in the CDC, (ii) $|\cos\theta| < 0.80$ and (iii) $p_\perp > 150$ MeV/c. A vertex was fitted to each pair and the χ^2-probability was required to be greater than 2%. The vertex was required to be displaced from the IP by at least 5 standard deviations, which accepted V^0 candidates with fight lengths as low as 2 mm. Candidates were rejected if their vertex was located outside of the VXD but included a track with more than one VXD hit. In the plane perpendicular to the beam, the angle between the vector sum of the momenta of the two charged tracks and the line joining the IP to the secondary vertex was required to be less than $k \cdot (2 + 20/p_\perp + 5/p_\perp^2)$ mrad and less than 60 mrad. Here, $p_\perp$ is in units of *GeV/c* and the coefficient k =1.75 for $\Lambda^0/\bar{\Lambda}^0$ candidates and 2.5 for K_s^0 candidates. For $\Lambda^0/\bar{\Lambda}^0$ candidates, a minimum vector-sum momentum of 500 *MeV/c* was required.

Cinematically-overlapping $\Lambda^0/\bar{\Lambda}^0$'s were removed from the K_s^0 sample by requiring $|\cos\theta^*| < 0.8$, where θ^* is the helicity angle between the positively charged track and the V^0 fight direction in the $\pi^+\pi^-$ rest frame, resulting in a 20% loss of the K_s^0 signal.

This cut also removed the photon-conversion background from the K^0_s sample.

Cinematically-overlapping K^0_s were rejected from the Λ^0 sample only for candidates whose vector-sum momentum was below 1.8 *GeV/c,* as above this momentum the "misidentified" K^0_s contributes a uniform background to the $p\pi$ invariant mass distribution. This was done by rejecting all $\Lambda^0/\bar{\Lambda}^0$ candidates whose $\pi\pi$ invariant mass was within 3σ and 30 MeV/c^2 of the K^0_s mass. This removed approximately 30% of the sample. Photon conversions were removed from the $\Lambda^0/\bar{\Lambda}^0$ sample by requiring that the proton helicity angle satisfy $\cos\theta^* \geq -0.95$. This removed approximately 2.5% of the $\Lambda^0/\bar{\Lambda}^0$ signal, assuming the $\Lambda^0/\bar{\Lambda}^0$ to be unpolarized.

The remaining V^0 candidates were divided into bins of momentum. In each bin the numbers of observed K^0_s and Λ^0 were derived from the $\pi\pi$ and $p\pi$ invariant mass distributions, respectively, where the faster track was assigned the proton mass. These numbers were divided by reconstruction efficiencies, estimated from the detector simulation, to yield production rates for each momentum bin. The reconstruction efficiencies are shown as a function of momentum in Fig. 4. As a check, the K^0_s and Λ^0 lifetimes were measured to be $c\tau_{K^0_S}$ = 2,62 $\pm$ 0.07(stat.) cm and $c\tau_{\Lambda^0}$=7.25 $\pm$ 0.38(stat.) cm, respectively, in good agreement with world average values [16].

6 Results for the Flavor-Inclusive Sample

The measured production per hadronic event $1/N_{evt}(dn_h/dx_p)$ for the five particle species *h* are shown as a function of scaled momentum $x_p = 2p/W$ in Fig. 5. For the charged species, these were obtained by multiplying the measured fractions by the total charged hadron production $1/N_{evt}(dn_{\pi+K+p}/dx_p)$ generated by the JETSET 7.4 simulation program, which provides a good description of data at the Z^0 [17]. The production of charged kaons is consistent with that of neutral kaons. The production ratios $K{:}\pi$ and $\Lambda{:}p$ show similar momentum dependence.

7 Flavor-Dependent Analysis

The analysis was repeated separately on the light- and *b*- tagged samples described in Section 2, and on the remaining sample of events assigned to neither sample, which

we denote as the *c*- tagged sample. The measured production rates r_k^m of each hadron species in each momentum bin for these three samples, k = light-tagged, c-tagged, *b*- tagged, were unfolded by inverting the relations:

$$r_k^m = \frac{\Sigma_l b_{lk} \epsilon_{lk} R_l r_l}{\Sigma_l \epsilon_{lk} R_l} \tag{1}$$

to yield true production rates r_l in events of the three flavor types, $l = Z^0 \rightarrow u\bar{u}, d\bar{d}, s\bar{s}$, $Z^0 \rightarrow c\bar{c}$, and $Z^0 \rightarrow b\bar{b}$. Here, R_l is the fraction of hadronic Z^0 decays of flavor type *l*, taken from the Standard Model, ϵ_{lk} is the event tagging efficiency matrix and b_{lk} represents the momentum-dependent bias of tag *k* toward selecting events of flavor *l* that contain hadrons of the type in question. The diagonal bias values [9, 15] are within a few percent of unity for the charged hadrons, reflecting a small multiplicity dependence of the flavor tags, and as much as 10% away for the neutrals, since tracks from unidentified neutrals can have large impact parameter. The off-diagonal bias values are somewhat larger, but they have little effect on the unfolded results. In Fig. 6 are shown the unfolded production rates per unit x_p for the five hadron species in light-flavor events. The errors are essentially the same as those in Fig. 5, those on the charged species being dominated by the correlated systematic uncertainty in the particle identification efficiencies. Systematic uncertainties in the unfolding procedure were estimated by varying the elements of the event tagging efficiency matrix ϵ by ± 0.01 and the values of the bias terms b_{lk} by $\pm 20\%$ of their deviation from unity, The unfolding systematic are typically small compared with the statistical errors. Qualitatively there is little difference between these rates in light-flavor events and those in the inclusive sample (Fig. 5). However the former rates are 7% lower for pions and kaons at 3 GeV/c, fall off more slowly with increasing momentum, and are more relevant for comparison with QCD predictions based on the assumption of massless quarks, as well as for testing the predictions of fragmentation models.

In Fig. 7 we show the ratios of production in *b*- flavor to light-flavor events for the five species. The systematic errors on the particle identification largely cancel in the ratio, and the total errors are predominantly statistical. There is higher production of charged pions in *b*- flavor at low momentum, with an approximately constant ratio for $0.02 < x_p < 0.07$. The production of both charged and neutral kaons is approximately equal in the two samples at $x_p = 0.02$, but the relative production in b-flavor events then increases with x_p, peaking at $x_p \approx 0.07$. There is approximately equal production of

baryons in b-flavor and light-flavor events below $x_p = 0.15$. For $x_p > 0.07$, production of pions, kaons and protons falls off faster in *b*- flavor events. These features are consistent with expectations based on the known production and decay characteristics of heavy hadrons. Also shown in Fig. 7 are the predictions of the JETSET7.4 and HERWIG5.7 event generators, both of which reproduce these features qualitatively. The exact values of these ratios depend on details of the *B* and *D* hadron production energy spectrum and decay modelling, and so provide information complementary to that in Fig. 6.

8 Summary and Conclusions

Using the SLD Cherenkov Ring Imaging Detector, we have made preliminary measurements of charged pion, kaon and proton production over most of the available momentum range in hadronic Z^0 decays, complementing previous measurements based on ionization energy loss. The production of K^0 and $\Lambda^0/\bar{\Lambda}^0$ was also measured. Our results for the flavor-inclusive sample are in agreement with those from previous measurements.

By isolating high-purity light- and *b*- tagged samples, we have produced the first measurements of identified hadron production in light-flavor events, which are appropriate for testing predictions of QCD calculations based on massless quarks and of fragmentation models. Production of these hadrons was also measured in *b*- flavor events and found to differ significantly from that in light-flavor events, being substantially higher for pions and kaons with $p < 5$ GeV/c, and falling much more rapidly wit h moment urn for pions, kaons and protons with $p > 5$ GeV/c. These differences are consistent with the known properties of *B* hadron production and decay.

Acknowledgements

We thank the personnel of the SLAC accelerator department and the technical staffs of our collaborating institutions for their outstanding efforts on our behalf.

References

[1] Y.L. Dokshitzer, V.A. Khoze, A.H. Mueller and S.I. Troyan, *Basics of Perturbative QCD*, Editions Frontieres, Gif-sur-Yvette, France (1991).

[2] M.D. Hildreth *et al.*, IEEE Trans. Nucl. Sci. **42** (1994) 451.

[3] C. J. S. Damerell *et al.*, Nucl. Inst. Meth. **A288** (1990) 288.

[4] K. Abe *et al.*, Nucl. Inst. Meth. **A343** (1994) 74.

[5] SLD Collab., K. Abe *et al.*, Phys. Rev. Lett. **73** (1994) 25.

[6] S. Brandt *et al.*, Phys. Lett. **12** (1964) 57.
E. Farhi, Phys. Rev. Lett. **39** (1977) 1587.

[7] SLD Collab., K. Abe *et al.*, Phys. Rev. **D53** (1996) 1023.

[8] K. Abe *et al.*, Nucl. Instr. and Meth. **A371** (1996) 195

[9] T.J. Pavel, Ph. D. Thesis, Stanford University, in preparation.

[10] DELPHI Collab., P. Abreu *et al.*, Nucl. Phys. **B444** (1995) 3.

[11] OPAL Collab., P.D. Acton *et al.*, Z. Phys. **C63** (1994) 181.

[12] ALEPH Collab., D. Decamp *et al.*, Z. Phys. **C66** (1995) 355.

[13] T. Sjöstrand, Comp. Phys. Comm. **82** (1994) 74.

[14] G. Marchesini *et al.*, Comp. Phys. Comm. **67** (1992) 465.

[15] K.G. Baird, Ph. D. Thesis, Rutgers University, December 1995; SLAC-R-483.

[16] Particle Data Group, Phys. Rev. **D50** (1994) 1173.

[17] ALEPH Collab., D. Decamp *et al.*, Z. Phys. **C55** (1992) 209.

**List of Authors

K. Abe,[19] K. Abe,[29] I. Abt,[13] T. Akagi,[27] N.J. Allen,[4] W.W. Ash,[27]†
D. Aston,[27] K.G. Baird,[24] C. Baltay,[33] H.R. Band,[32] M.B. Barakat,[33]
G. Baranko,[9] O. Bardon,[15] T. Barklow,[27] A.O. Bazarko,[10] R. Ben-David,[33]
A.C. Benvenuti,[2] G.M. Bilei,[22] D. Bisello,[21] G. Blaylock,[6] J.R. Bogart,[27]
B. Bolen,[17] T. Bolton,[10] G.R. Bower,[27] J.E. Brau,[20] M. Breidenbach,[27]
W.M. Bugg,[28] D. Burke,[27] T.H. Burnett,[31] P.N. Burrows,[15] W. Busza,[15]
A. Calcaterra,[12] D.O. Caldwell,[5] D. Calloway,[27] B. Camanzi,[11] M. Carpinelli,[23]
R. Cassell,[27] R. Castaldi,[23][a] A. Castro,[21] M. Cavalli-Sforza,[6] A. Chou,[27]
E. Church,[31] H.O. Cohn,[28] J.A. Coller,[3] V. Cook,[31] R. Cotton,[4]
R.F. Cowan,[15] D.G. Coyne,[6] G. Crawford,[27] A. D'Oliveira,[7] C.J.S. Damerell,[25]

M. Daoudi,[27] R. De Sangro,[12] R. Dell'Orso,[23] P.J. Dervan,[4] M. Dima,[8]
D.N. Dong,[15] P.Y.C. Du,[28] R. Dubois,[27] B.I. Eisenstein,[13] R. Elia,[27]
E. Etzion,[4] D. Falciai,[22] C. Fan,[9] M.J. Fero,[15] R. Frey,[20] K. Furuno,[20]
T. Gillman,[25] G. Gladding,[13] S. Gonzalez,[15] G.D. Hallewell,[27] E.L. Hart,[28]
J.L. Harton,[8] A. Hasan,[4] Y. Hasegawa,[29] K. Hasuko,[29] S. J. Hedges,[3]
S.S. Hertzbach,[16] M.D. Hildreth,[27] J. Huber,[20] M.E. Huffer,[27] E.W. Hughes,[27]
H. Hwang,[20] Y. Iwasaki,[29] D.J. Jackson,[25] P. Jacques,[24] J. A. Jaros,[27]
A.S. Johnson,[3] J.R. Johnson,[32] R.A. Johnson,[7] T. Junk,[27] R. Kajikawa,[19]
M. Kalelkar,[24] H. J. Kang,[26] I. Karliner,[13] H. Kawahara,[27] H.W. Kendall,[15]
Y. D. Kim,[26] M.E. King,[27] R. King,[27] R.R. Kofler,[16] N.M. Krishna,[9]
R.S. Kroeger,[17] J.F. Labs,[27] M. Langston,[20] A. Lath,[15] J.A. Lauber,[9]
D.W.G.S. Leith,[27] V. Lia,[15] M.X. Liu,[33] X. Liu,[6] M. Loreti,[21] A. Lu,[5]
H.L. Lynch,[27] J. Ma,[31] G. Mancinelli,[22] S. Manly,[33] G. Mantovani,[22]
T.W. Markiewicz,[27] T. Maruyama,[27] H. Masuda,[27] E. Mazzucato,[11]
A.K. McKemey,[4] B.T. Meadows,[7] R. Messner,[27] P.M. Mockett,[31]
K.C. Moffeit,[27] T.B. Moore,[33] D. Muller,[27] T. Nagamine,[27] S. Narita,[29]
U. Nauenberg,[9] H. Neal,[27] M. Nussbaum,[7] Y. Ohnishi,[19] L.S. Osborne,[15]
R.S. Panvini,[30] H. Park,[20] T.J. Pavel,[27] I. Peruzzi,[12][b] M. Piccolo,[12]
L. Piemontese,[11] E. Pieroni,[23] K.T. Pitts,[20] R.J. Plano,[24] R. Prepost,[32]
C.Y. Prescott,[27] G.D. Punkar,[27] J. Quigley,[15] B.N. Ratcliff,[27] T.W. Reeves,[30]
J. Reidy,[17] P.E. Rensing,[27] L.S. Rochester,[27] P.C. Rowson,[10] J.J. Russell,[27]
O.H. Saxton,[27] T. Schalk,[6] R.H. Schindler,[27] B.A. Schumm,[14] S. Sen,[33]
V.V. Serbo,[32] M.H. Shaevitz,[10] J.T. Shank,[3] G. Shapiro,[14] D.J. Sherden,[27]
K.D. Shmakov,[28] C. Simopoulos,[27] N.B. Sinev,[20] S.R. Smith,[27] M.B. Smy,[8]
J.A. Snyder,[33] P. Stamer,[24] H. Steiner,[14] R. Steiner,[1] M.G. Strauss,[16] D. Su,[27]
F. Suekane,[29] A. Sugiyama,[19] S. Suzuki,[19] M. Swartz,[27] A. Szumilo,[31]
T. Takahashi,[27] F.E. Taylor,[15] E. Torrence,[15] A.I. Trandafir,[16] J.D. Turk,[33]
T. Usher,[27] J. Va'vra,[27] C. Vannini,[23] E. Vella,[27] J.P. Venuti,[30] R. Verdier,[15]
P.G. Verdini,[23] S.R. Wagner,[27] A.P. Waite,[27] S.J. Watts,[4] A.W. Weidemann,[28]
E.R. Weiss,[31] J.S. Whitaker,[3] S.L. White,[28] F.J. Wickens,[25] D.A. Williams,[6]
D.C. Williams,[15] S.H. Williams,[27] S. Willocq,[33] R.J. Wilson,[8]
W.J. Wisniewski,[27] M. Woods,[27] G.B. Word,[24] J. Wyss,[21] R.K. Yamamoto,[15]
J.M. Yamartino,[15] X. Yang,[20] S.J. Yellin,[5] C.C. Young,[27] H. Yuta,[29]
G. Zapalac,[32] R.W. Zdarko,[27] C. Zeitlin,[20] and J. Zhou,[20]

[1] *Adelphi University, Garden City, New York 11530*
[2] *INFN Sezione di Bologna, I-40126 Bologna, Italy*
[3] *Boston University, Boston, Massachusetts 02215*
[4] *Brunel University, Uxbridge, Middlesex UB8 3PH, United Kingdom*
[5] *University of California at Santa Barbara, Santa Barbara, California 93106*
[6] *University of California at Santa Cruz, Santa Cruz, California 95064*
[7] *University of Cincinnati, Cincinnati, Ohio 45221*
[8] *Colorado State University, Fort Collins, Colorado 80523*
[9] *University of Colorado, Boulder, Colorado 80309*

[10] *Columbia University, New York, New York 10027*
[11] *INFN Sezione di Ferrara and Università di Ferrara, I-44100 Ferrara, Italy*
[12] *INFN Lab. Nazionali di Frascati, I-00044 Frascati, Italy*
[13] *University of Illinois, Urbana, Illinois 61801*
[14] *Lawrence Berkeley Laboratory, University of California, Berkeley, California 94720*
[15] *Massachusetts Institute of Technology, Cambridge, Massachusetts 02139*
[16] *University of Massachusetts, Amherst, Massachusetts 01003*
[17] *University of Mississippi, University, Mississippi 38677*
[19] *Nagoya University, Chikusa-ku, Nagoya 464 Japan*
[20] *University of Oregon, Eugene, Oregon 97403*
[21] *INFN Sezione di Padova and Università di Padova, I-35100 Padova, Italy*
[22] *INFN Sezione di Perugia and Università di Perugia, I-06100 Perugia, Italy*
[23] *INFN Sezione di Pisa and Università di Pisa, I-56100 Pisa, Italy*
[24] *Rutgers University, Piscataway, New Jersey 08855*
[25] *Rutherford Appleton Laboratory, Chilton, Didcot, Oxon OX11 0QX United Kingdom*
[26] *Sogang University, Seoul, Korea*
[27] *Stanford Linear Accelerator Center, Stanford University, Stanford, California 94309*
[28] *University of Tennessee, Knoxville, Tennessee 37996*
[29] *Tohoku University, Sendai 980 Japan*
[30] *Vanderbilt University, Nashville, Tennessee 37235*
[31] *University of Washington, Seattle, Washington 98195*
[32] *University of Wisconsin, Madison, Wisconsin 53706*
[33] *Yale University, New Haven, Connecticut 06511*
† *Deceased*
[a] *Also at the Università di Genova*
[b] *Also at the Università di Perugia*

Figure captions

1. Identification efficiencies for charged pions measured with tracks from K^0_s and τ decays in the data (solid symbols). The open symbols are for the same analysis of simulated samples. The circles are for the liquid analysis and the squares for the gas analysis.

2. Identification efficiencies for $\pi^\pm, K^\pm$, and $p/\bar{p}$. The widths of the shaded bands represent the estimated systematic uncertainties, which are completely correlated between momenta.

3. Preliminary charged hadron production fractions in hadronic Z^0 decays. The circles represent the $\pi^\pm$ fraction, the squares the $K^\pm$ fraction, and the triangles the $p/\bar{p}$ fraction. Open symbols are from the liquid analysis; solid symbols are from the gas analysis. The dashed and dotted lines are the predictions of the JETSET7.4 and HERWIG5.7 fragmentation models, respectively.

4. The efficiency for reconstructing and selecting K^0 and Λ^0 decays in selected hadronic events. The efficiencies include the relevant branching ratios and the effects of detector acceptance.

s. Preliminary production rates per event per unit scaled momentum, $x_p = 2p/W$, for $\pi^\pm$ (dots), $K^\pm$ (squares), K^0 (open squares), $p/\bar{p}$ (triangles), and $\Lambda^0/\bar{\Lambda}^0$ (open triangles) in inclusive hadronic Z^0 decays. The $p/\bar{p}$ and $\Lambda^0/\bar{\Lambda}^0$ rates have been scaled by 0.1 for clarity. The errors are statistical and systematic added in quadrature. The systematic errors on the charged species are dominant and are correlated point to point. An overall normalization uncertainty of 4% on the neutral species is not included.

6. Preliminary production rates per light-flavor event per unit scaled momentum for $\pi^\pm$ (dots), $K^\pm$ (squares), K^0 (open squares), $p/\bar{p}$ (triangles), and $\Lambda^0/\bar{\Lambda}^0$ (open triangles). The $p/\bar{p}$ and $\Lambda^0/\bar{\Lambda}^0$ rates have been scaled by 0.1 for clarity. The errors are statistical and systematic added in quadrature. The systematic errors on the charged species are dominant and are correlated point to point. An overall normalization uncertainty of 4% on the neutral species is not included.

7. The ratio of production rates in *b* events to that in light flavor events. The dashed and dotted lines are the predictions of the JETSET7.4 and HERWIG5.7 fragmentation models, respectively.

Figure 1: Identification Efficiency Calibration

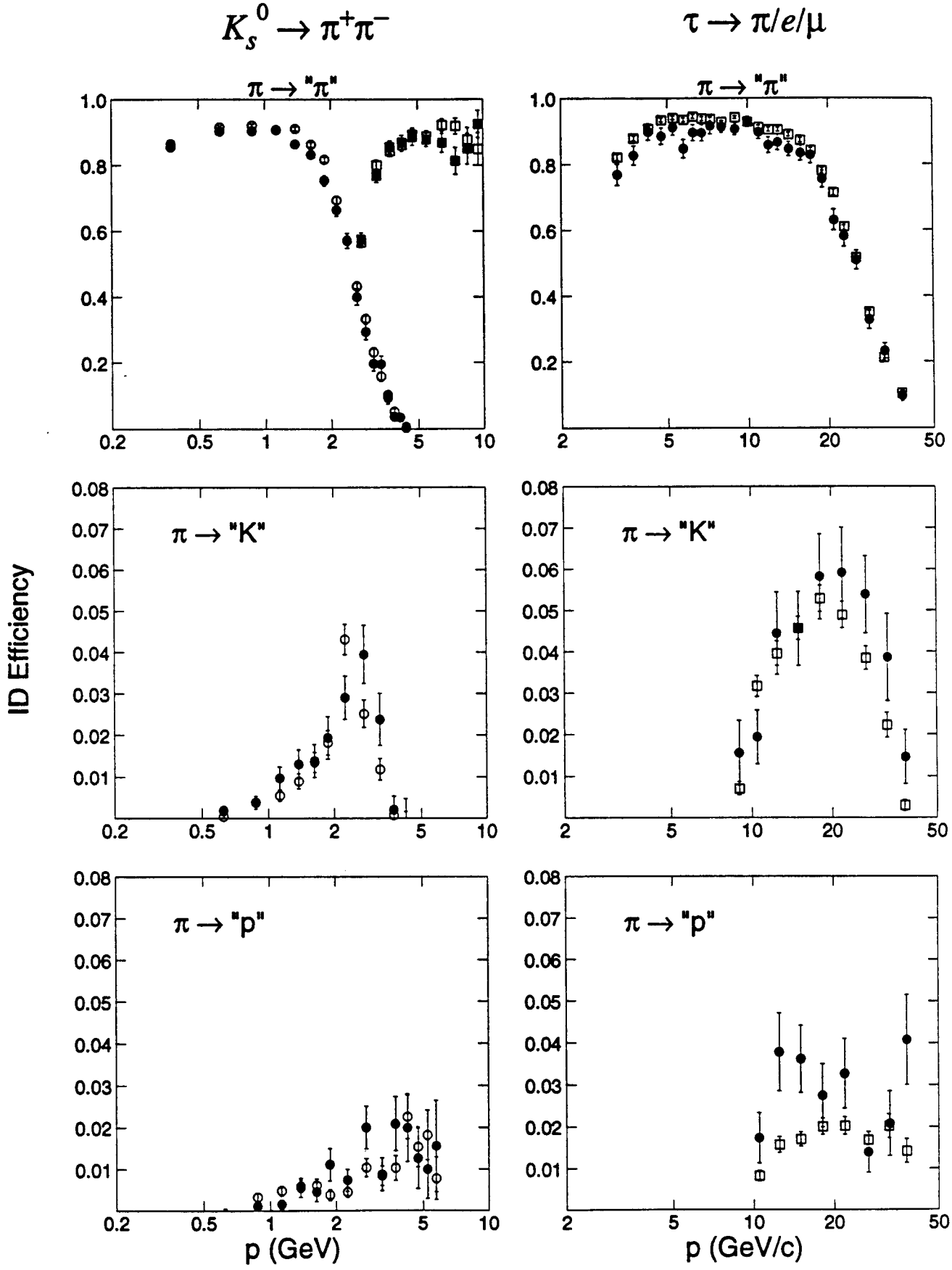

Figure 2: Identification Efficiencies

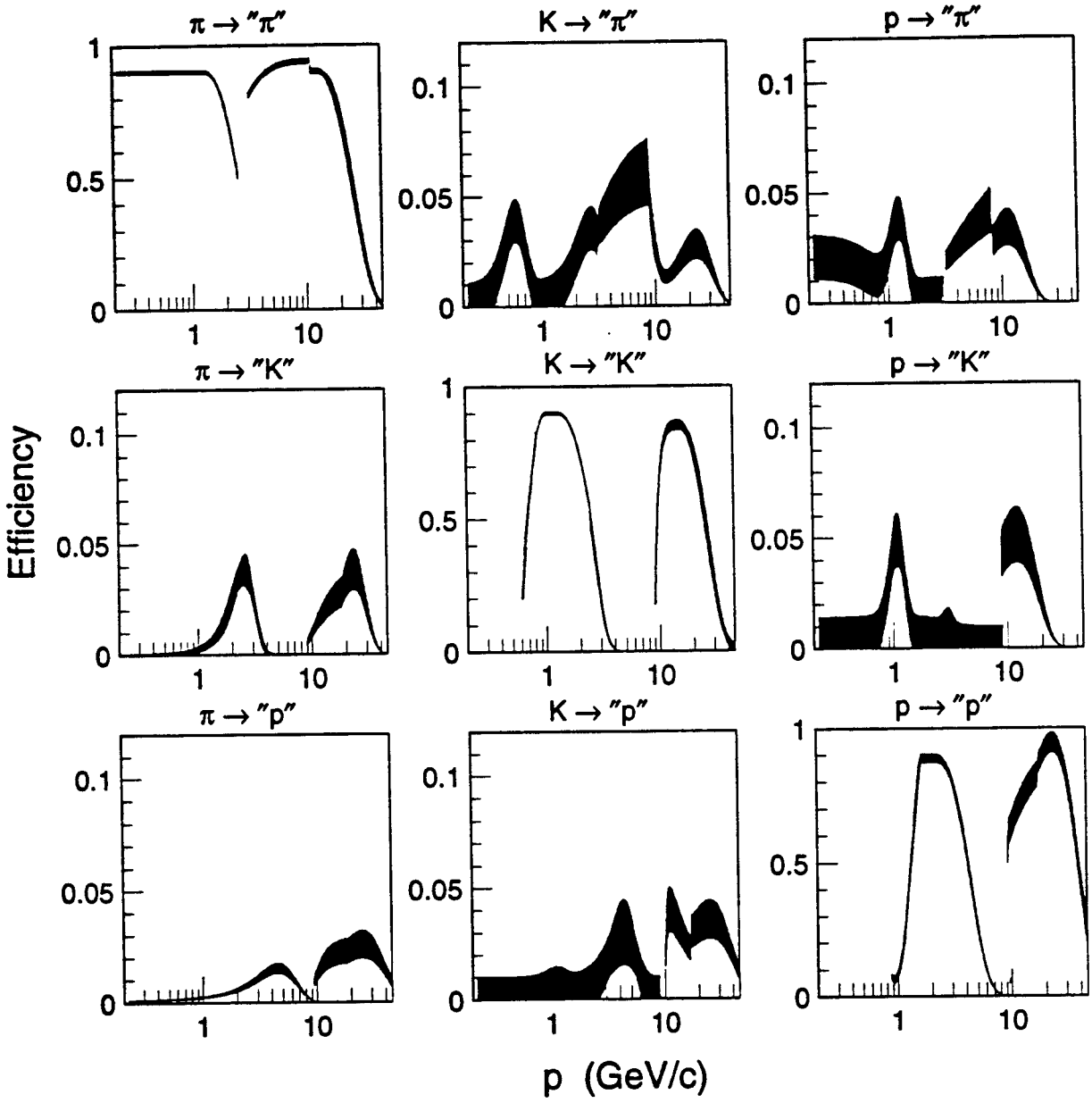

Figure 3: Fraction of $\pi/K/p$ in Z^0 Decays

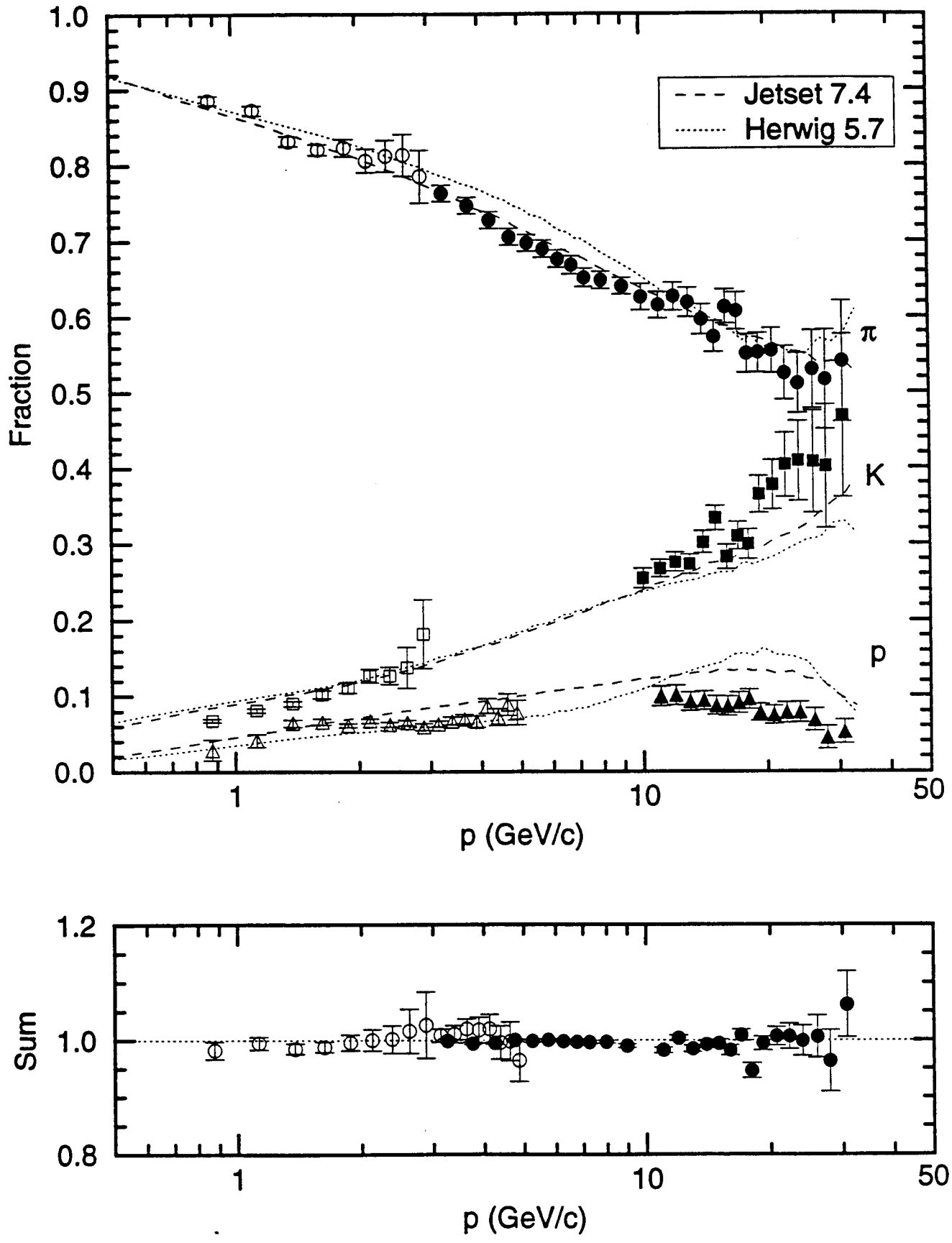

Figure 4 : V^0 Reconstruction Efficiencies

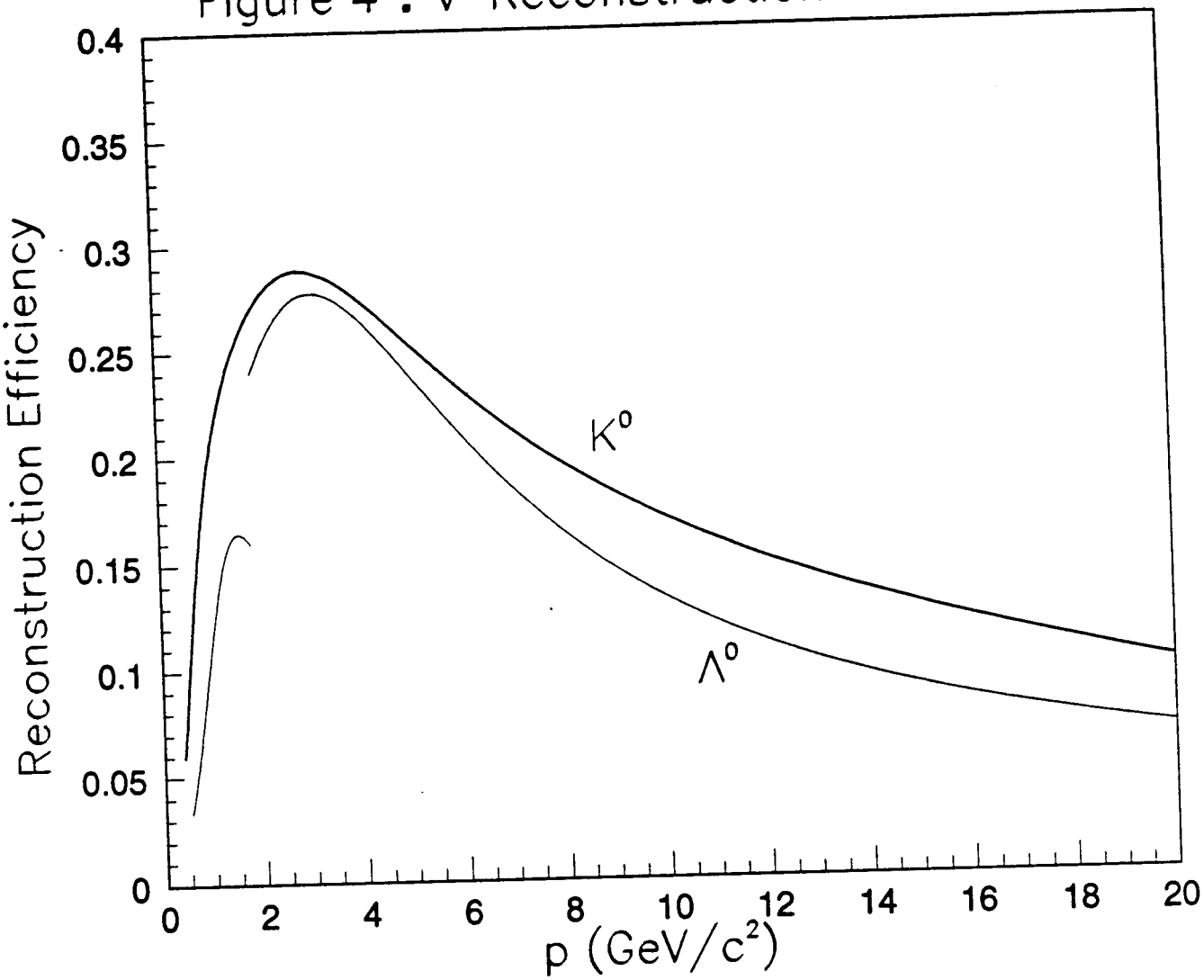

Figure 5: Hadronic Spectra in Z^0 Decays

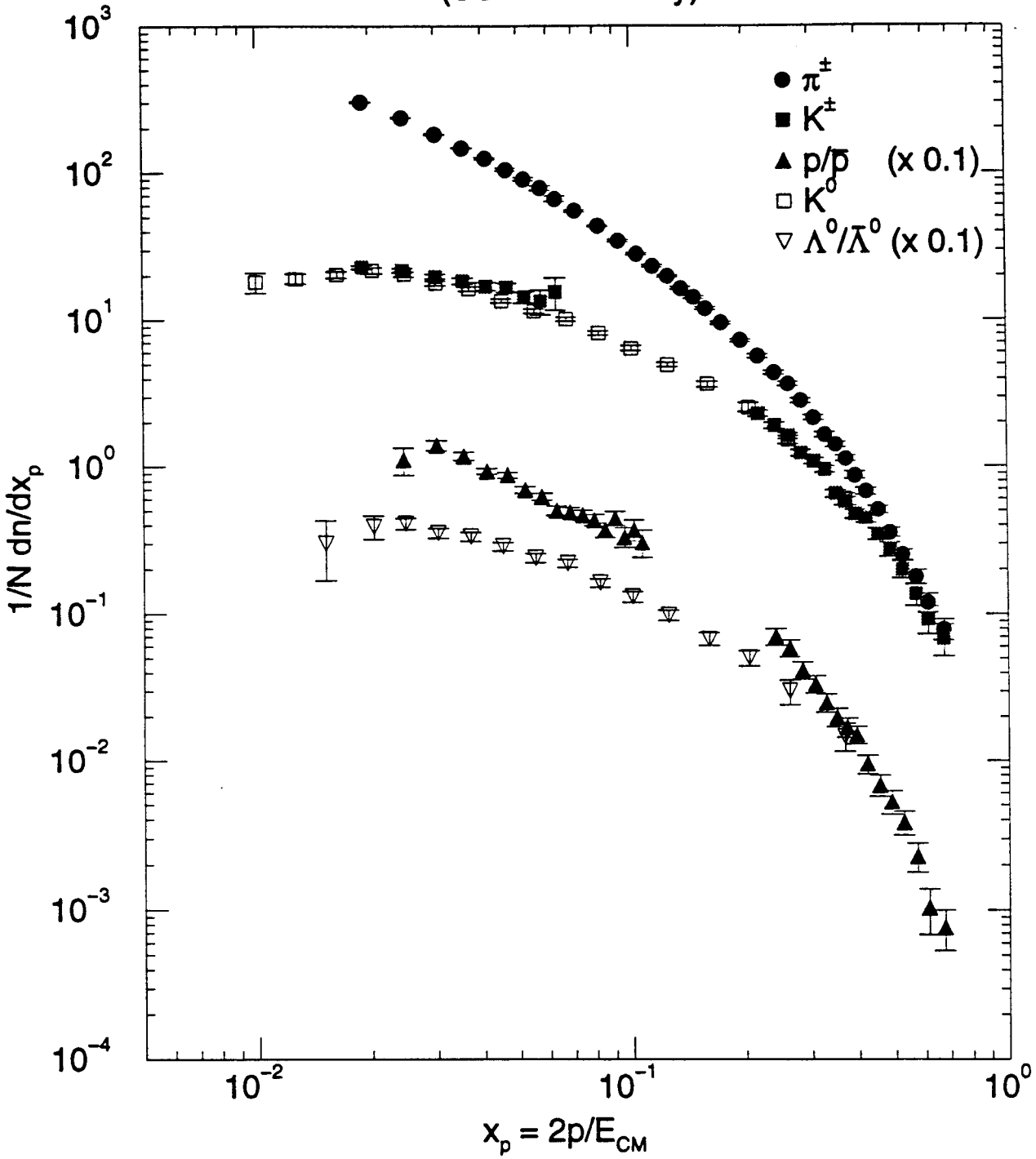

Figure 6: Hadronic Spectra in $Z^0 \rightarrow uu,dd,ss$ Decays

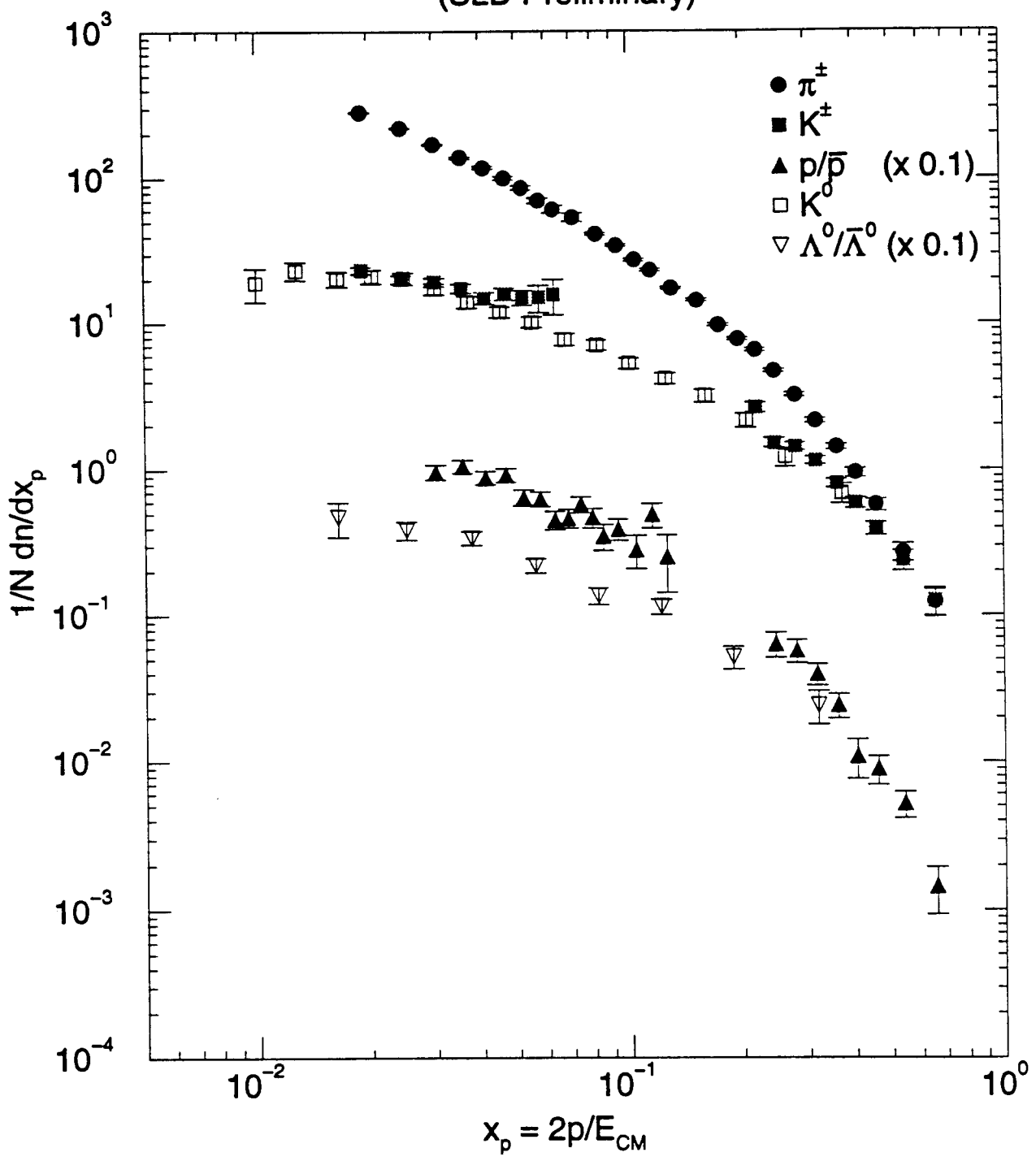

Figure 7: *b/uds* Production Ratio

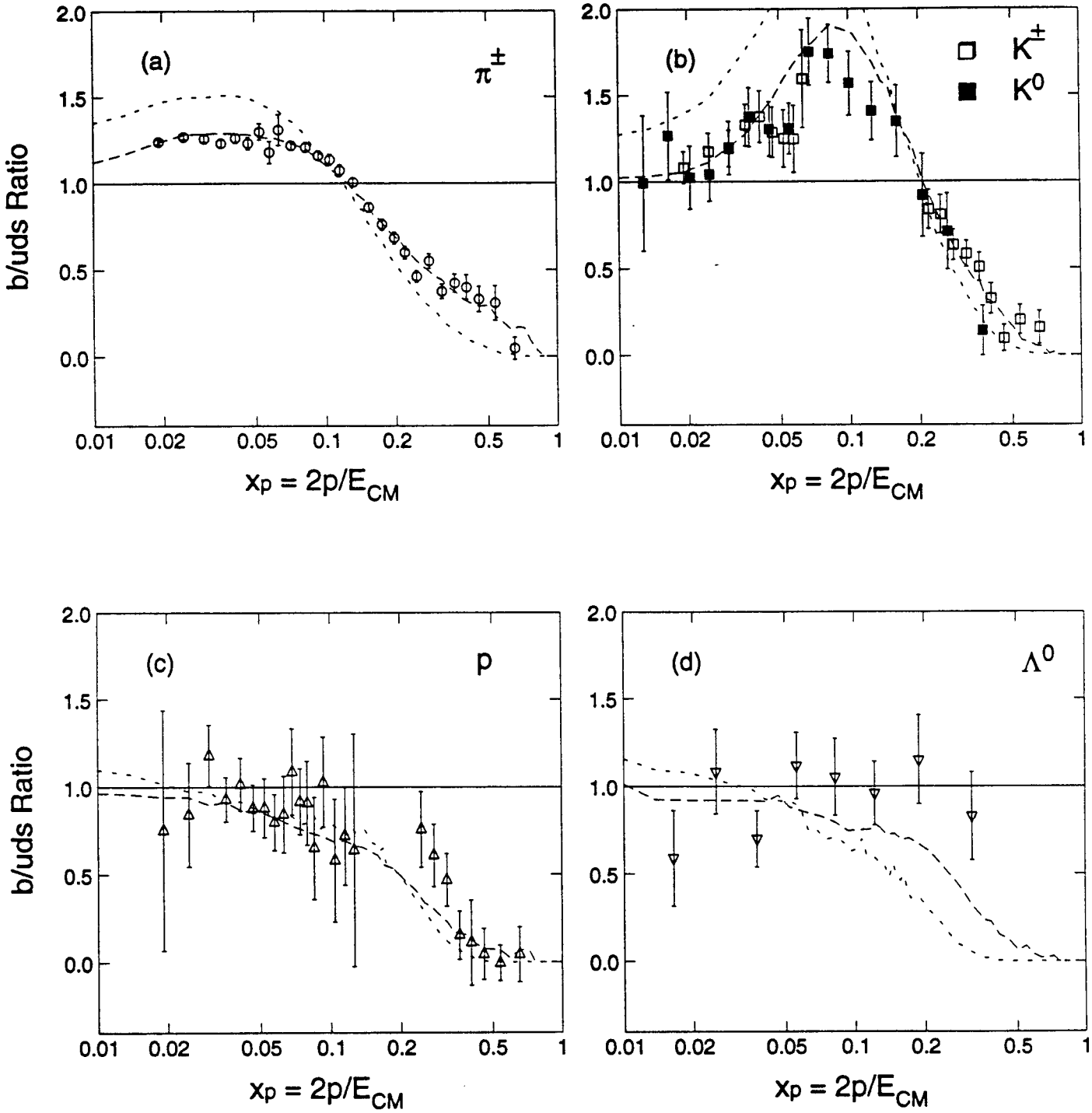

Figure 5: Hadronic Spectra in Z^0 Decays

(SLD Preliminary)

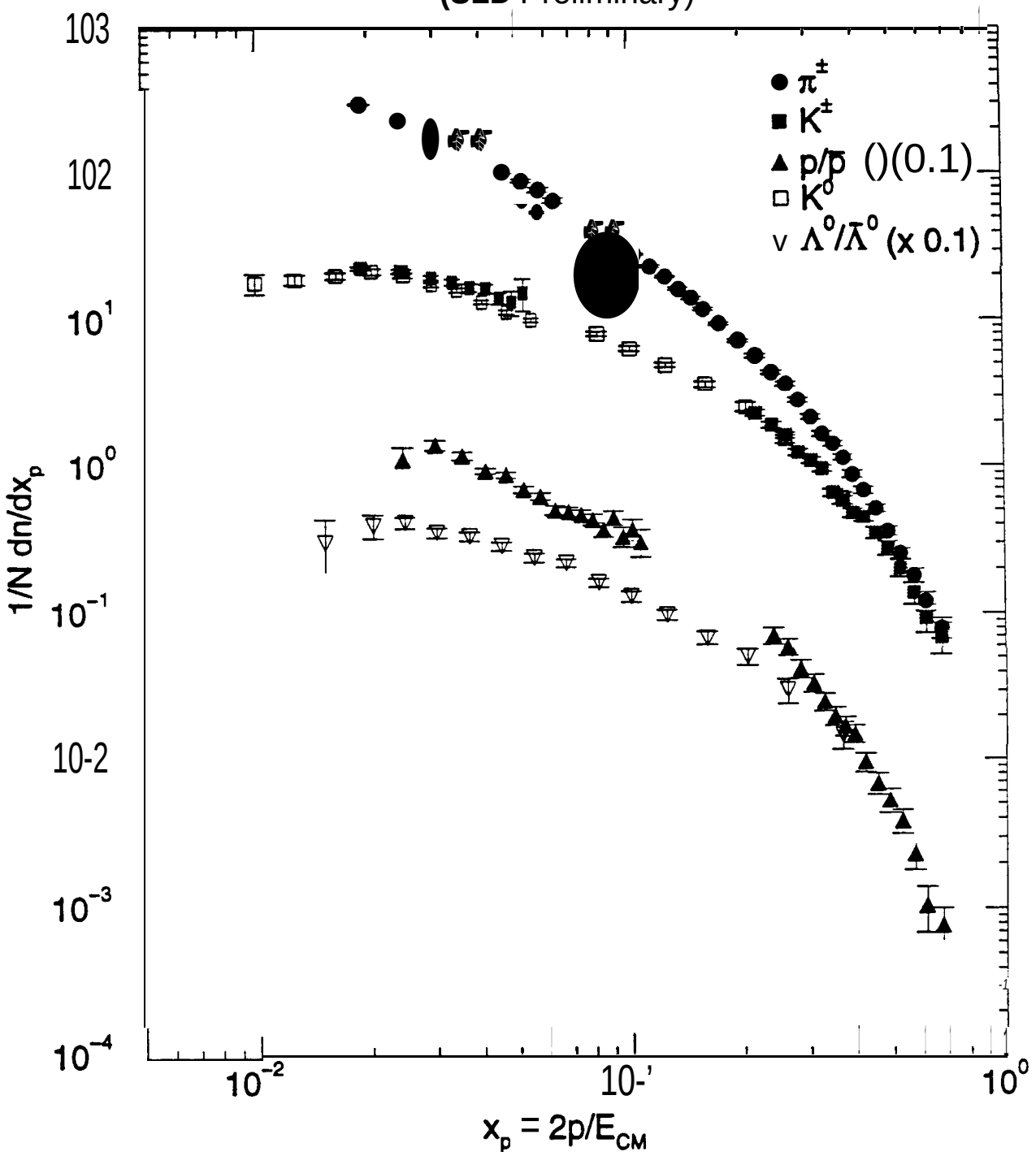

Figure 1: Identification Efficiency Calibration

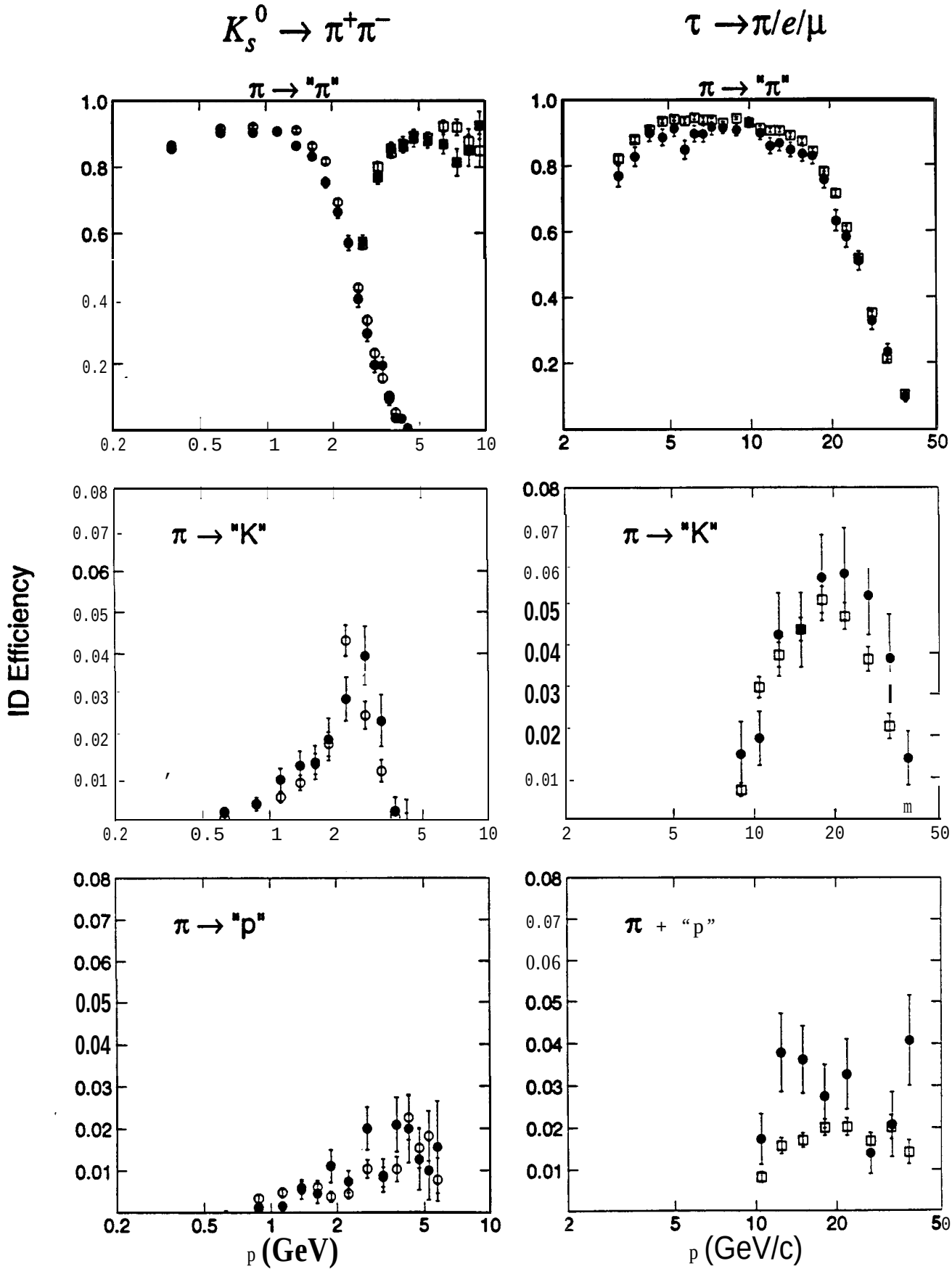

Figure 3: Fraction of π/K/p in Z* Decays

(SLD Preliminary)